UC San Diego
UC San Diego Previously Published Works

Title

Structure and Dynamics in Mg2+-Stabilized γ-Na3PO4

Permalink

https://escholarship.org/uc/item/42d3z6f2

Journal

Journal of the American Chemical Society, 143(41)

ISSN

0002-7863

Authors

Cheung, Emily A

Nguyen, Han

Tang, Hanmei

et al.

Publication Date

2021-10-20

DOI

10.1021/jacs.1c06905

Peer reviewed

Structure and Dynamics in Mg^{2+}-Stabilized γ-Na$_3$PO$_4$

Emily A. Cheung, Han Nguyen, Hanmei Tang, Anton P. J. Stampfl, Maxim Avdeev, Ying Shirley Meng,* Neeraj Sharma,* and Nicolas R. de Souza*

ABSTRACT: In parallel with advances in the synthesis of solid-state ionic conductors, there is a need to understand the underlying mechanisms behind their improved ionic conductivities. This can be achieved by obtaining an atomic level picture of the interplay between the structure of materials and the resultant ionic diffusion processes. To this end, the structure and dynamics of Mg^{2+}-stabilized rotor phase material γ-Na$_3$PO$_4$, characterized by neutron scattering, are detailed in this work. The Mg^{2+}-stabilized rotor phase is found to be thermally stable from 4 to 650 K. However, signatures of orientational disorder of the phosphate anions are also evident in the average structure. Long-range Na$^+$ self-diffusion was probed by quasi-elastic neutron scattering and subsequently modeled via a jump diffusion matrix with consideration of the phosphate anion rotations. The resultant diffusion model points directly to coupled anion–cation dynamics. Our approach highlights the importance of considering the whole system when developing an atomic level picture of structure and dynamics, which is critical in the rational design and optimization of energy materials.

Energy transfer (µeV)
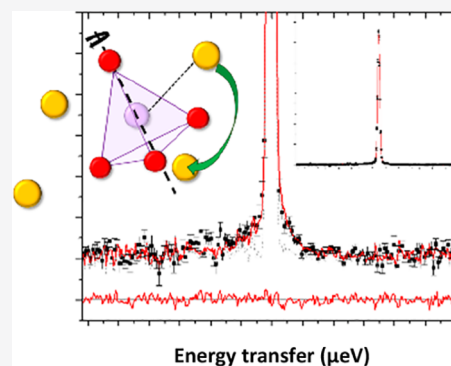
1. INTRODUCTION

Solid-state ionic conductors have attracted significant interest on account of their potential applications as solid-state electrolytes. One class of materials that has been investigated in this respect are the rotor phase materials.[1−3] These typically feature complex anions which, although translationally fixed, have a high rotational dynamic disorder. It is postulated that the anion reorientations lower the activation energy barrier to the diffusion of alkali metal cations through the material via a "paddle-wheel" mechanism.[3−6]

Sodium orthophosphate (Na$_3$PO$_4$) is an example of an inorganic rotor phase material. It has two phases separated by a reversible first-order phase transition at 598 K[7−9]—a poorly conducting low-temperature tetragonal α-phase (space group $P\bar{4}2_1c$)[9] and a high-temperature cubic γ-phase (space group $Fm\bar{3}m$[8−10] or $F432$[11]). Depending on how the material has been synthesized, γ-Na$_3$PO$_4$ has been reported to have an ionic conductivity of up to 5 mS/cm at temperatures close to 600 K.[7,12,13] A number of studies have shown that γ-Na$_3$PO$_4$ may be stabilized at ambient temperatures by aliovalent substitution on the Na$^+$ site.[12−15] In addition, modifications of the form Na$_{3−2x}$M$_x$PO$_4$, where M is a divalent cation, have been reported to have higher ionic conductivities in comparison to pure γ-Na$_3$PO$_4$.[14,16,17]

Difficulties in synthesizing pure γ-Na$_3$PO$_4$ as well as the intrinsic disorder of the anion framework itself have resulted in several proposed structural models. Although these differ in the choice of the atom(s) fixed on a special position, the underlying structure of each model is the same, that is, a face-centered-cubic phosphate framework where all tetrahedral

and octahedral interstices are occupied by sodium cations.[8−11,18] In this way, γ-Na$_3$PO$_4$ presents an interesting case of ionic conduction through a densely packed lattice, where the Na$^+$ diffusion processes may be correlated to the phosphate rotations. Quasi-elastic neutron scattering (QENS) has previously been used to investigate the rotational diffusion of the PO$_4^{3−}$ anions in pure Na$_3$PO$_4$.[5] A separate QENS study of Na$^+$ self-diffusion in both pure γ-Na$_3$PO$_4$ (between 773 and 1073 K) and solid solution xNa$_2$SO$_4$·$(1 − x)$Na$_3$PO$_4$ has also been reported.[19] The proposed models for both the pure and solid solution systems suggest that Na$^+$ diffusion is dominated by jumps between sites with tetrahedral coordination.[19] However, the possible interplay between the phosphate framework dynamics and long-range sodium diffusion have not previously been examined. In addition, there has not previously been a direct experimental characterization of the Na$^+$ diffusion mechanism in cation stabilized γ-Na$_3$PO$_4$.

Atomic-scale dynamics of sodium-based ionic conductors can be challenging to probe experimentally although significant theoretical work has been conducted in this space. A common approach is the use of diffraction and Fourier or bond valence sum analysis to indicate possible sodium pathways. However, diffraction provides a static picture from which diffusion and

dynamics can only be inferred indirectly. Electrochemical impedance spectroscopy (EIS) is often used to infer dynamics, but it is a bulk technique; the resulting data typically reflect multiple processes, e.g., bulk versus grain boundary conduction. While solid-state NMR provides valuable information about atomic level dynamics, it is sensitive to one element per experimental setup, e.g., ^{23}Na. Thus, for materials where there is an interplay of multiple diffusion processes, it is difficult to gain an overall view of the dynamics from a single experiment. In this respect, NMR and QENS have long been recognized as complementary.[20]

Inelastic neutron scattering, specifically QENS in the present context, is unique in that it measures the dynamics of all atoms or atomic units in a given energy window and both their individual and concerted motions. There are, however, few atomic level descriptions of Na$^+$ diffusion or dynamics from QENS-based studies. The vast majority of the QENS-based diffusion works are based on investigations following protons, as fortuitously protons are overwhelmingly incoherent neutron scatterers which simplifies the analysis of QENS data, and therefore they are widely explored in the literature. The scarcity in QENS studies of Na$^+$ conductors is because the Na scatters both incoherently and coherently, and the explicit separation of these contributions is nontrivial. As such, this work represents a new, practical approach to identify the weighted contributions of different Na$^+$ diffusion processes in experimental QENS data, which can be applied more broadly to other materials featuring mixed scatterers.

Recent work focused on Na-based ionic conductors has highlighted the importance of the link between framework dynamics and ionic diffusion in NASICON and Na$_3$PS$_4$[21−25] but has mostly focused on theoretical calculations. This work therefore provides an experimental demonstration of the possibility of considering the coupling with long-range sodium diffusion with framework dynamics. This is critical both in fundamental understanding and also for practical optimization in energy storage devices. Specifically, research interest in concerted displacement[6] is addressed, where this work explicitly combines crystallography and the jump matrix formulation to model the directly evidenced experimental observations of paddle-wheel-type concerted diffusion.

Here, the focus is on Mg^{2+}-stabilized γ-Na$_3$PO$_4$ of the form Na$_{3−2x}$Mg$_x$PO$_4$, with particular emphasis on a synthetic target of $x = 0.128$. Both high-resolution neutron powder diffraction and X-ray powder diffraction were used to model the average structure. The insight gained from the structural characterization was used to model the Na$^+$ long-range diffusion processes, which were probed directly by using quasi-elastic neutron scattering.

2. EXPERIMENTAL METHODS

Powder Na$_3$PO$_4$ (Sigma-Aldrich, 96%) was dried in a muffle furnace at 200 °C for 48 h and then allowed to cool to 100 °C and transferred to an argon-filled glovebox. Polycrystalline samples of Na$_{3−2x}$Mg$_x$PO$_4$, with target compositions $x = 0.064$ and $x = 0.128$, were prepared via solid-state reaction following similar methods outlined by Irvine et al.[12,14] Stoichiometric amounts of Na$_2$CO$_3$ (Sigma-Aldrich, 99.99%), (NH$_4$)$_2$HPO$_4$ (Sigma-Aldrich, 99.99%), and MgO (Alfa Aesar, 99.95%) were ground with an agate mortar and pestle before being ball milled with ethanol for 24 h. The mixture was subsequently sintered in a sequence of three heating steps—650 °C for 1 h, followed by 800 °C for 2 h and finally 1000 °C for 48 h—with intermediate regrinding.

Initial laboratory X-ray powder diffraction (XRD) patterns were collected for all three samples on a PANalytical X'Pert Pro Multipurpose powder diffractometer using Cu Kα radiation. High-resolution neutron powder diffraction (NPD) patterns of the $x = 0.064$ and $x = 0.128$ compositions were measured on Echidna[26,27] at the Australian Nuclear Science and Technology Organisation (ANSTO). The powders were packed in a 9 mm diameter vanadium can and measured at 4 and 300 K by using a wavelength of 1.6215(5) Å. To verify the structure of the two end compositions ($x = 0$ and $x = 0.128$), complementary diffraction patterns at 300 and 650 K were measured on the Powder Diffraction beamline[28] at the Australian Synchrotron. For these measurements, the powders were packed into a quartz capillary and measured by using a wavelength of 0.68955(12) Å. For all collected patterns, the structures of the respective samples were modeled via Rietveld analysis using GSAS/EXPGUI.[29,30] The background in the NPD data was modeled by using a 28-term Chebyshev polynomial as implemented in GSAS.

Quasi-elastic neutron scattering (QENS) experiments were performed on the high-resolution backscattering spectrometer Emu[31] at ANSTO on the $x = 0.128$ sample. The powder sample was packed into an aluminum sample can with annular geometry (10 mm total sample thickness). Inelastic spectra of the sample were measured at 400, 500, 550, 600, and 650 K over an energy range ±31 μeV at a final wavelength of 6.27 Å. The inelastic spectrum measured on a standard vanadium cylinder was used as the resolution function and for detector efficiency and solid-angle corrections. The inelastic spectrum of an empty cryostat was similarly measured and used for background subtraction. All analysis was performed on background-subtracted and normalized data and excluded any detector traces which coincided with Bragg reflections.

3. RESULTS AND DISCUSSION

3.1. Structural Characterization. Powder diffraction patterns were measured for Na$_{3−2x}$Mg$_x$PO$_4$ with $x = 0$, 0.064, and 0.128. At 300 K, both the $x = 0$ and $x = 0.064$ compositions were found to be a mixture between the tetragonal α-Na$_3$PO$_4$ phase (space group $P\bar{4}2_1c$) and cubic γ-Na$_3$PO$_4$ phase (space group $Fm\bar{3}m$). The Rietveld refined fits of the average structure model to the data for these compositions are shown in the Supporting Information. For the $x = 0.128$ composition, however, Rietveld analysis of both the NPD and synchrotron XRD patterns at 300 K showed that the cubic γ-Na$_3$PO$_4$ phase is stabilized, with no observable reflections from the tetragonal phase and only a minor MgO impurity phase (weight fraction 0.8(2)%) present (Figure 1). This suggests that a minimum Mg^{2+} doping level is required for the stabilization of the γ-phase at ambient temperature. In addition, NPD data at 4 K and synchrotron XRD data at 650 K show that the γ-phase in the $x = 0.128$ composition is stable throughout the entire temperature range measured. The crystallographic details of the final model fitted to the NPD data at 4 K are summarized in Table 1, where the octahedral and tetrahedral Na sites are labeled as Na1 and Na2, respectively. For this composition, the cubic phase was modeled with space group $F432$ as models using the $Fm\bar{3}m$ space group were found to be inadequate to account for the intensities of several reflections (see the Supporting Information).

Successful doping of Mg is evidenced by the combination of changes in lattice parameters, overall composition for $x = 0.128$ of Na$_{2.68}$Mg$_{0.147}$PO$_4$ ($\chi^2 = 1.51$, $R_p = 2.62\%$, $wR_p = 3.34\%$) with free refinement of Na and Mg SOFs, and weight fraction of MgO from 1.62(3)% and 0.8(3)% between the $x = 0.064$ and 0.128 compositions, respectively. However, it should be noted that the Mg SOFs shown in Table 1 are low due to the multiplicity of the crystallographic site (96j). Refining these
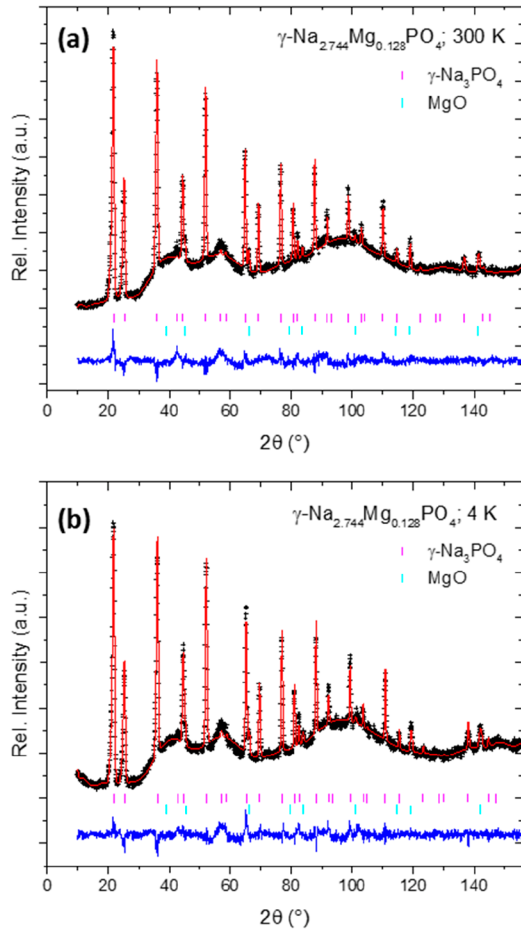
Figure 1. Rietveld refined fit of structural models to the NPD pattern of $Na_{3-2x}Mg_xPO_4$, $x = 0.128$, measured at (a) 300 K and (b) 4 K with a wavelength of 1.6215(5) Å. The data are shown as black crosses, the calculated Rietveld model as a red line, and the difference between the data and the calculated model as a blue line. Reflection markers of γ-Na_3PO_4 and MgO are shown as vertical lines in magenta and cyan, respectively.

short-range structural disorder. Future work will be targeted at total scattering experiments to elucidate the local structure of these materials and correlate to the background observed in the NPD data. A large contributor to this background is likely to be the orientational disorder of the phosphate anions. Previous work on γ-Na_3PO_4 has shown that the phosphate anions undergo a uniaxial rotation about the P−O1 axis, which is aligned in the ⟨100⟩ direction, i.e., directed toward an octahedral Na site.[5,11,32,33] This rotation occurs on the picosecond time scale and corresponds to orientational disorder of the O2, O3, and O4 oxygens (Figure 2a,b). From the crystal structure, the preferential alignment of the uniaxial rotation axis means that there are six possible orientations of the phosphate anion (Figure 2c).[3,11] As such, the uniaxial rotation axis disorder may be dynamic, and the reorientation of the phosphate anion is expected to occur on the nanosecond time scale.[34] The relevance of these rotations to Na^+ dynamics is that as proposed by Wilmer et al.,[33] each of the phosphate anions is bound to one sodium cation from a tetrahedral site. Therefore, it follows that any bound sodium necessarily participates in the phosphate rotations.

In view of these local rotations, it is expected that long-range jump diffusion pathways involving phosphate-bound sodium would not be energetically equivalent to pathways between sodium that do not participate in the phosphate rotations. As such, it is necessary to distinguish between these two types of tetrahedral sodium sites. The structural model from our Rietveld analysis of the PD data labels all tetrahedral Na as a single site type (Na2 in Table 1) and therefore does not have the sensitivity to make this distinction. However, starting from the primitive unit cell, the crystal structure features three sodium Bravais sublattices—one where sodium occupies a site with octahedral coordination and two sublattices where sodium is in a tetrahedral site—which from here can be labeled as O, T1, and T2, respectively. Lacking any evidence from our diffraction patterns that could indicate a super-structure where the phosphate bound sodium is exclusively from either T1 or T2 type sites, as a starting premise, phosphate binding to sodium may occur in either tetrahedral sublattice at sites, which from here will be termed T1R and T2R. This leads to two possible distinct configurations, viz. random distributions of sodium−phosphate binding sites (Figure 3). In the first configuration, the phosphate bound sodiums are taken equally from the two tetrahedral sublattices. Considering that there are four sodium sites in each sublattice per unit cell, this results in a 2:2 ratio between T1R and T2R

SOFs often leads to errors that are comparable to the refined quantities; therefore in this work, the Mg concentration was fixed to the input synthetic ratio and used as such in the rest of the work.

An interesting feature of the NPD patterns is the Q-dependent diffuse scattering background, which is indicative of

Table 1. Crystallographic Details of $Na_{3-2x}Mg_xPO_4$ with Target Composition $x = 0.128$ as Determined from Rietveld Analysis of Structural Models Using Neutron Powder Diffraction Data Measured at 4 K

name	site	x	y	z	SOF	U_{iso} (×100), Å^2
P	4a	0	0	0	1	3.77(6)
O1	24e	0	0	−0.2132[c]	0.303	7.46(11)
O2	96j	−0.154[c]	0.120[c]	−0.002[c]	0.0303	1.0[c]
O3	96j	0.041[c]	−0.197[c]	0.062[c]	0.0303	1.261[c]
O4	96j	0.08[c]	0.168[c]	0.08[c]	0.0303	4.4(4)
Na1[a]	96j	0.5174	0.4885	0.5124	0.0381	10.41(22)
Mg1[a]	96j	0.5174	0.4885	0.5124	0.0018	10.41(22)
Na2[b]	96j	0.2586	0.2398	0.2706	0.0762	4.94(9)
Mg2[b]	96j	0.2586	0.2398	0.2706	0.0036	4.94(9)

[a]SOF = site occupation factors. [b]Constrained to be on the same site. [c]Initially refined and then fixed; space group = $F432$; 38 refinement parameters; χ^2 = 1.54; R_p = 2.68%; wR_p = 3.39%; a = 7.37060(11) Å.
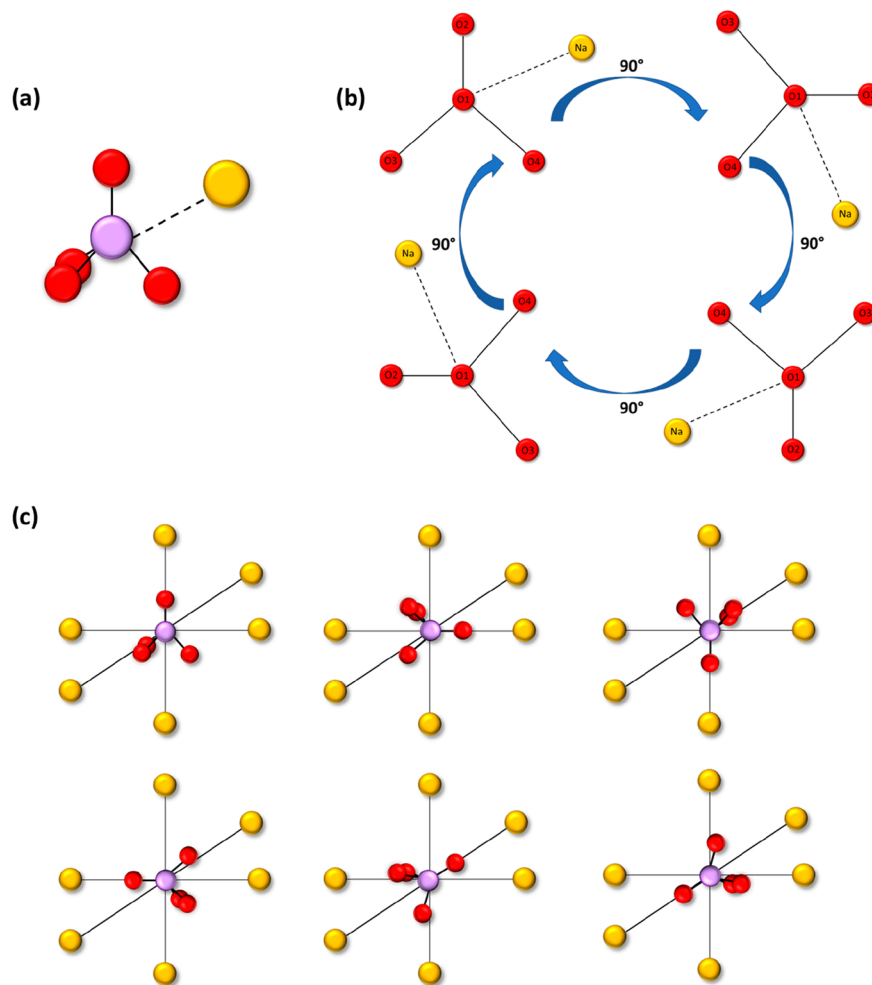
Figure 2. (a) Visual representation of a phosphate bound to a sodium (also referred to in text as a PO$_4$Na unit). The phosphorus, oxygen, and sodium atoms are shown in purple, red, and yellow, respectively. (b) Schematic of the fast, uniaxial phosphate rotation. (c) Schematic of the six possible orientations of the phosphate anion. The reorientation of the phosphate anion through these positions is described by the slow phosphate rotation.

sites and therefore will be termed the 2:2 configuration. The second possibility is to split the phosphate bound sodiums unevenly between the two tetrahedral sublattices such that there is a 3:1 ratio between T1R and T2R sites. From here, this will be termed the 3:1 configuration. A full derivation of these two possible configurations is provided in the Supporting Information.

To gain insight into the possible sodium long-range diffusion mechanism, difference Fourier maps were generated from a fit of the structural model with the sodium occupancy set to zero to the NPD data at 4 and 300 K and the synchrotron XRD data at 650 K (Figure 4). The maps indicate that at all temperatures sodium is localized on the crystallographic octahedral and tetrahedral sites. This result suggests that sodium diffusion can be modeled through jumps between nearest-neighbor sodium sites. Given that there is no indication of a preferred diffusion pathway from the diffraction data, as a starting point for modeling the diffusion mechanism, jumps between any sites should *a priori* be considered to participate in long-range diffusion.

3.2. Na$^+$ Long-Range Self-Diffusion Probed by QENS. A temperature-dependent quasi-elastic neutron scattering study was conducted on the high-resolution cold back-

scattering spectrometer Emu to gain direct insight into the diffusion mechanism in γ-Na$_{3-2x}$Mg$_x$PO$_4$, x = 0.128, at an atomic level. Broadening of the elastic line relative to the measured resolution function was observed at all measured temperatures (400−650 K). The spectra at all temperatures were well described by a simple empirical model consisting of a linear combination of a flat background, a delta function, and a single Lorentzian function (Figure 5). In the time scale accessible in this study, it is possible that the QENS broadening results from the slow phosphate/sodium rotation or sodium long-range diffusion.[19,34] However, the Q dependence of the QENS broadening is suggestive of long-range diffusion.[20,35,36] For this reason, analysis started from the characterization of the sodium long-range diffusion rather than phosphate/sodium rotational diffusion.

As sodium is a mixed coherent and incoherent neutron scatterer ($\sigma_{incoherent}$:$\sigma_{coherent}$ = 1.62(3):1.66(2),[37] where σ is the bound scattering cross section measured in barns), the quasi-elastic part of the dynamic scattering function includes contributions from both self-diffusion (incoherent scattering) and collective diffusion (coherent scattering). In full, this is written as the sum of at least two Lorentzian functions. However, only one Lorentzian function could be resolved in
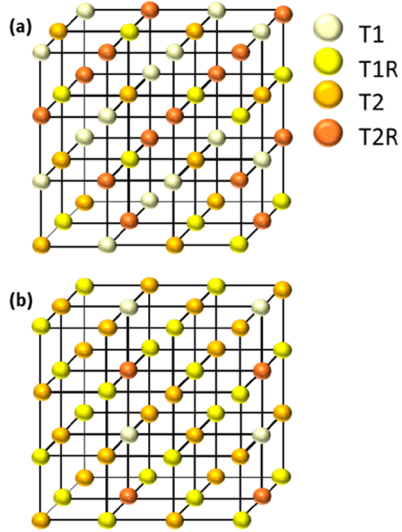
Figure 3. Schematic showing the tetrahedral sodium sites under the (a) 2:2 configuration (T1R:T2R = 2:2) and (b) 3:1 configuration (T1R:T2R = 3:1). Each box represents the tetrahedral sublattices from a single unit cell.

the fit of the empirical model to the data, indicating that, here, only one contribution can be resolved. For diffusion on lattices it is well established that the amplitudes and broadenings from coherent and incoherent QENS differ by the site blocking factor $(1 - c)$, where c is the concentration of the diffusing species (here, Na).[38−41] Thus, for γ-Na$_{2.744}$Mg$_{0.128}$PO$_4$, where c = 0.91, the relative contributions from incoherent and coherent scattering are on considerably different scales. Moreover, particularly in the low-temperature region (400−550 K), the quasi-elastic amplitude $(A_1(Q))$ is approximately constant. This indicates that the dominant contribution to the observed QENS broadening in this study is from incoherent scattering. Therefore, all modeling focused on Na$^+$ long-range self-diffusion.

The other important finding from the fit of the empirical model is the large elastic amplitude $(A_0(Q))$. It has previously been shown that purely coherent scatterers that only participate in rotational diffusion do not contribute to elastic scattering outside of the Bragg peaks.[42] As such, the $A_0(Q)$ here cannot be attributed solely to the phosphate anions. This indicates that within the sensitivity of the data a large fraction (f) of the sodium cations is localized. With the assumption that the diffuse scattering is Laue monotonic, approximate expressions for $A_0(Q)$ and $A_1(Q)$ were written in terms of the contributions of the phosphate framework (A_0^{frame}), sodium (A_{Na}), and f. Explicitly, this is given by

$$A_0(Q) \sim A_0^{frame} + fA_{Na} \tag{1}$$

and

$$A_1(Q) \sim (1 - f)A_{Na} \tag{2}$$

With this approach, f and the fitted amplitudes $A_0(Q)$ and $A_1(Q)$ can be related by combining eqs 1 and 2. From this, and by substituting the scattering cross sections for A_0^{frame} and A_{Na}, $f = 10/12$ is estimated for γ-Na$_{2.744}$Mg$_{0.128}$PO$_4$. This step is detailed in the Supporting Information.

Turning now to the detailed diffusion mechanism, it is important to note that sodium sites in γ-Na$_3$PO$_4$ do not form a single Bravais lattice. Therefore, to achieve a detailed description of the Na$^+$ diffusion, a long-range jump diffusion model was built by using a jump matrix construction.[43−45] Each element of the matrix precisely describes a jump from a site of type i to a site of type j and is dependent on the jump rate $1/\tau_{ij}$, where τ_{ij} is the residence time. As such, jumps that are forbidden $(\tau_{ij} \rightarrow \infty)$ result in a corresponding matrix element equal to zero. Consequently, the jump matrix construction is particularly amenable to selecting the sites that form part of the diffusion pathway(s). As simplifying assumptions to this model, here the small defect concentration (Mg^{2+} dopants) is neglected, and the random distribution of phosphate-bound sodium at the tetrahedral sites is approxi-
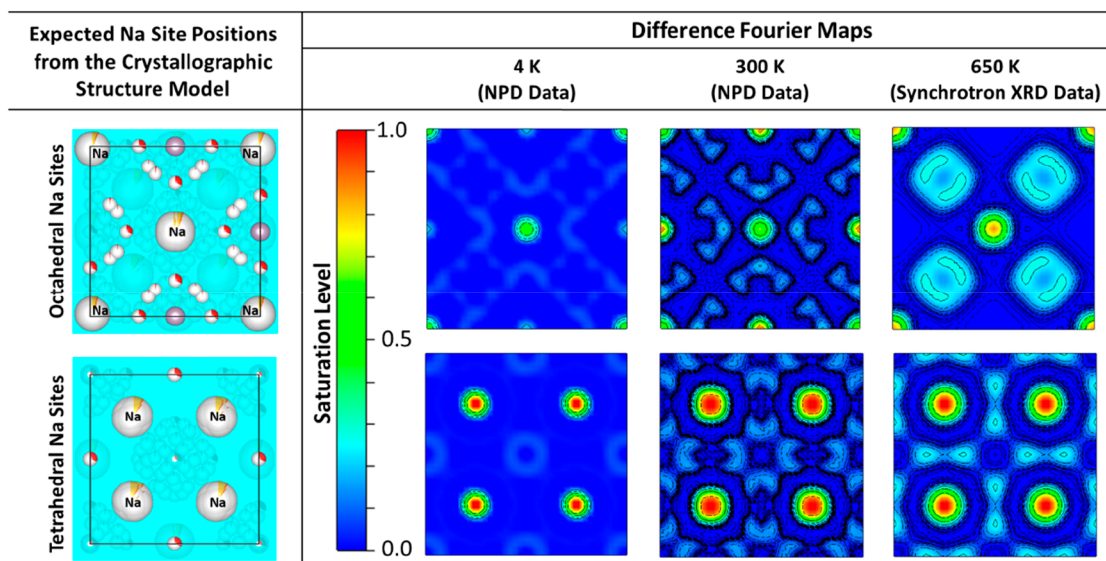

Figure 4. Difference Fourier maps of γ-Na$_{2.744}$Mg$_{0.128}$PO$_4$ showing slices through the Na site model positions at 4, 300, and 650 K. The maps were generated from fits of the structural model to the powder diffraction data where all Na occupancies were set to zero. The color scale for the difference Fourier maps shows regions with the greatest difference between the model and data in red and the least difference in blue (NPD data maximum saturation = 0.63; synchrotron data maximum saturation = 3.98).
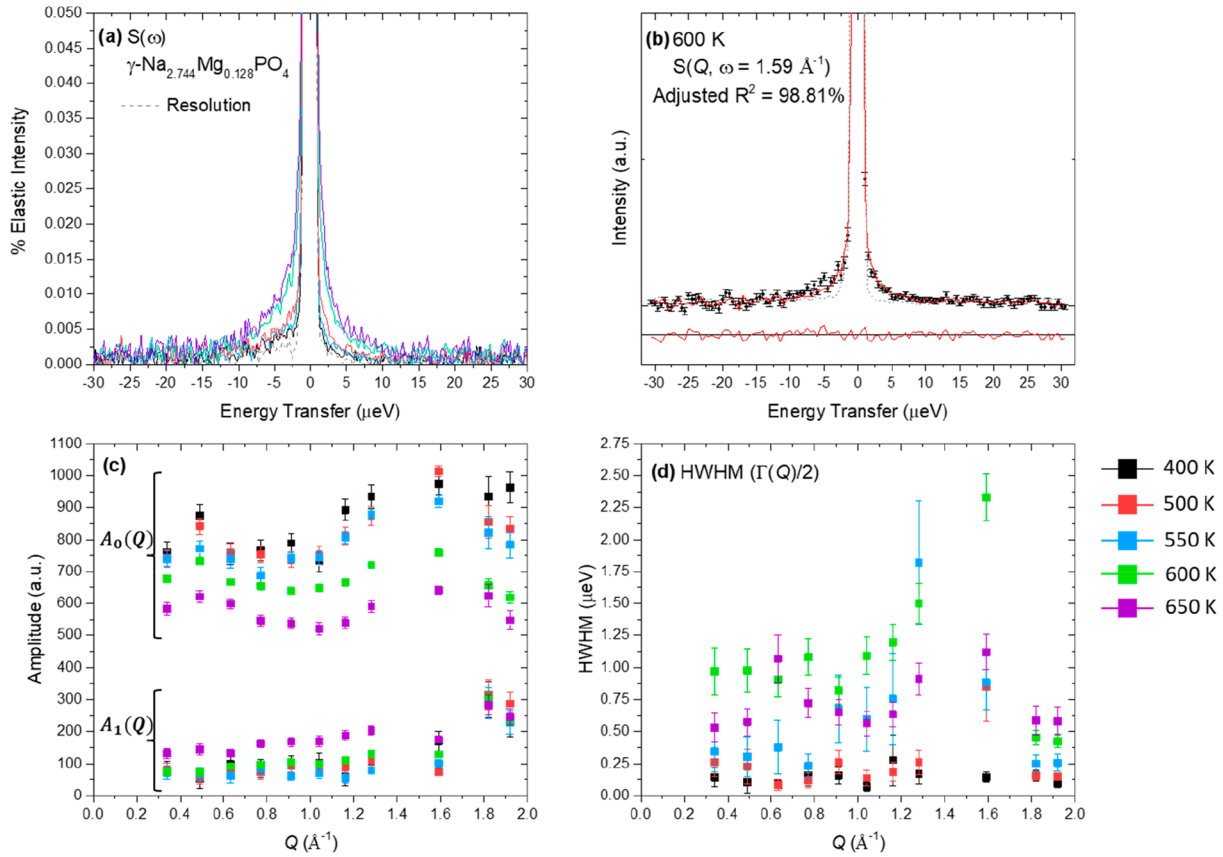
Figure 5. (a) Temperature dependence of the summed scattering function $S(\omega)$ for γ-$Na_{2.744}Mg_{0.128}PO_4$. (b) Representative fit to the QENS spectra with the simple empirical model. The data are shown in black, the fit of the model as a red line through the data, and the difference between the data and model as a red line below the data. (c) Amplitudes of the elastic and quasi-elastic components, $A_0(Q)$ and $A_1(Q)$, respectively, from the fit of the simple empirical model to the QENS spectra. (d) Q dependence of the line width (HWHM) of the Lorentzian function from the fit of the simple empirical model. Note: a single broadening term accounted for the line shape (a minimal model) which we used for the remainder of the analysis.

mated by a superposition of homogeneous tetrahedral sublattices.

For an estimated 2 out of 12 sodium cations per unit cell participating in long-range diffusion, there are only two possible diffusion pathways. These are dependent on the configuration of the sodium−phosphate binding (Figure 3). In the case that the cell is in the 2:2 configuration, diffusion proceeds via tetrahedral sites of the same kind, e.g., jumps between sites of type T1 only. In this way, since the jumps are between half of the sites from one Bravais sublattice, this may be visualized in the manner of a restricted Chudley−Elliott pathway[46] and therefore will be termed resCE. The second possibility is when the cell is in the 3:1 configuration. In this case, the pathway consists in jumps between sites of type T1 and T2R, which from here will be termed the T1T2R pathway. The details of the derivation of these models are provided in the Supporting Information.

The fitting model incorporating the scattering function derived from the jump matrix is given by

$$S(Q, \omega) = b(Q) + A_0^{frame}(Q)\delta(\omega) + A_{Na}\langle S_{Na}(\mathbf{Q}, \omega)\rangle_{\text{powder average}}$$
(3)

where $b(Q)$ is a Q-dependent background, $A_0^{frame}(Q)$ is the elastic scattering amplitude from the phosphate framework structure, A_{Na} is the total scattering amplitude from sodium, and $S_{Na}(Q,\omega)$ is the incoherent sodium scattering function for

either the resCE or T1T2R diffusion pathway. This was fitted to the spectra from each temperature data set in a simultaneous two-dimensional fit across energy transfer (ω) and Q. Despite having very different pathways (Figure 6) and diffusion constants (Table 2), both the resCE and T1T2R models fitted the data well, with the relative merit of each model indistinguishable based on the quality of fit. This suggested that, from the approach of modeling the QENS broadening over the momentum transfer range of this study, both the resCE and T1T2R pathways are plausible models. In addition, for both models, the sum of the amplitudes $A_0^{frame}(Q)$ and fA_{Na} agrees within error with the $A_0(Q)$ from the fit of the empirical model (see the Supporting Information), which further supports the validity of our proposed diffusion pathways.

However, the scattering function in eq 3 cannot explain the detailed Q dependence of the amplitudes $A_0(Q)$ and $A_1(Q)$ from the empirical model. This suggests the phosphate and phosphate-bound sodium rotations make a small contribution to the scattering amplitudes. Therefore, corrections to the scattering function were derived for the scenarios that the PO_4−Na units undergo either (i) the fast, uniaxial rotation only, which is expected at all temperatures, or (ii) both the fast, uniaxial rotation and the slow P−O axis reorientation, which may set in at higher temperatures. This was done by starting from the exact form for the structure factors for each rotation,
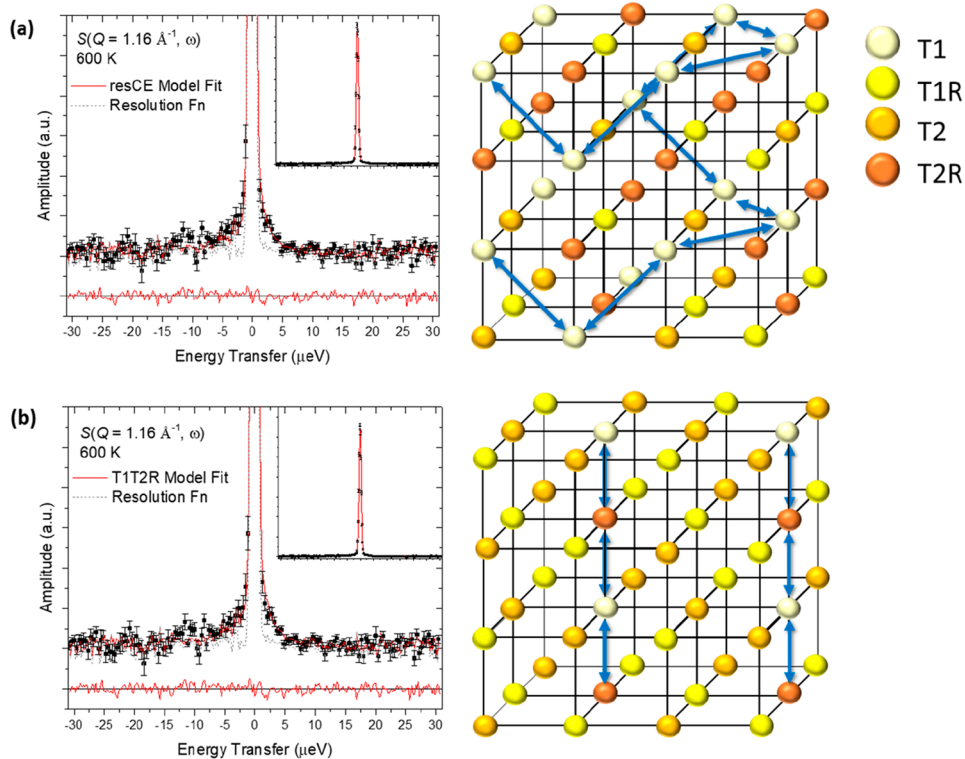
Figure 6. Representative fits of the (a) resCE (2:2 configuration) and (b) T1T2R (3:1 configuration) diffusion models to the QENS spectra and visual representation of their respective pathways. The data are shown in black, the fit of the model as a red line through the data, the difference between the data and the model as a red line below the data, and the measured resolution function as a dashed gray line.

Table 2. Summary of the Key Diffusion Parameters from the Fit of the resCE and T1T2R Models to the QENS Data

model	temp (K)	jump distance (Å)	residence time (ns)	diffusion coeff ($\times 10^{-7}$ cm^2/s)	adjusted R^2
resCE	400	5.26	4.1(7)	1.1(2)	0.9612
	500	5.28	2.5(4)	1.7(3)	0.9715
	550	5.28	1.2(2)	4.0(7)	0.9668
	600	5.29	0.63(3)	7.4(4)	0.9734
	650	5.30	0.66(3)	7.0(3)	0.9576
T1T2R	400	3.72	3.6(6)	0.6(1)	0.9613
	500	3.73	2.1(4)	1.1(2)	0.9716
	550	3.74	1.0(1)	2.3(7)	0.9671
	600	3.74	0.57(2)	4.1(1)	0.9739
	650	3.75	0.58(2)	4.1(1)	0.9577

yielding separate contributions from sodium and oxygen. As a simplifying assumption, dynamical correlations between oxygen and sodium were neglected. This step closely follows previous studies[5,33,47] on the phosphate framework dynamics and is detailed in the Supporting Information. The corrected scattering functions were thus finally written as the sum of the oxygen rotational processes and the sodium scattering function, which was modified by convolution of the sodium rotational and translational (jump matrix) processes with reference to the basis set formed by the primitive unit cell of γ-Na$_3$PO$_4$. Specifically, to conserve the number of sodium per basis set, it was considered that Na$^+$ may either be stationary or participate in one of three diffusion mechanisms—rotation only, translation only, or rotation−translation—depending on the sodium location and binding to phosphate at the T1R and

T2R sites. The conditions and derivation of the corrected scattering function are given in the Supporting Information.

Table 3. Summary of the Possible Diffusion Pathways Illustrated in Figure 7

cell configuration	sites included in the diffusion pathway	jump matrix model
2:2	T1 only	resCE
2:2	T1R only	resCE
3:1	T1 and T2R	T1T2R

Interestingly, as outlined in Table 3 and shown in Figure 7, examining the elastic and quasi-elastic amplitudes of the corrected scattering functions provides definite points of distinction between the possible diffusion pathways, which are not apparent from using the jump matrix model alone (eq 3). This makes it possible to identify which case corresponds to the data in this study, providing insight into the framework dynamics and its possible coupling with sodium long-range diffusion.

As shown in Figure 7a,b, scenarios i and ii correspond to very different relative magnitudes for the expected $A_0(Q)$ and $A_1(Q)$ amplitudes (see the Supporting Information). Compared to Figure 5, from 400 to 650 K, the elastic amplitude of the spectra measured in this study is significantly larger than the quasi-elastic amplitude, which indicates that the framework dynamics in this study is dominated by the phosphate anions participating in the fast rotation only (scenario i).

Identifying the preferred diffusion pathway finally proceeded via direct fits to the corresponding amplitudes of the corrected
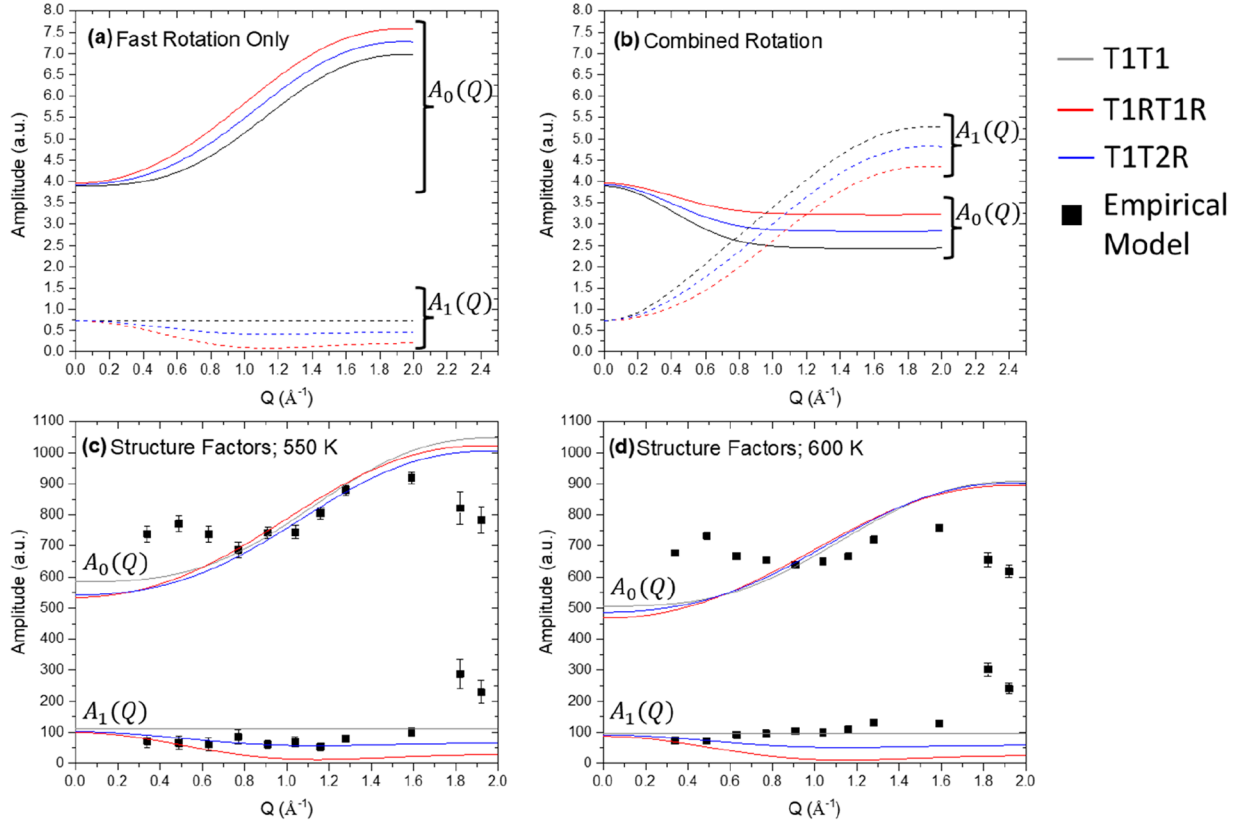
Figure 7. Calculated elastic and quasi-elastic amplitudes $A_0(Q)$ (solid lines) and $A_1(Q)$ (dashed lines) for the T1T1, T1RT1R, and T1T2R diffusion pathways for scenario i (fast rotation only) and scenario ii (combined rotation). Fits to the empirical $A_0(Q)$ and $A_1(Q)$ with scenario i at (c) 550 K and (d) 600 K. In all plots, the T1T1, T1RT1R, and T1T2R pathways are shown in gray, red, and blue, respectively.

scattering function, where the only fit parameter was a common scale factor. Lacking sufficient information about contributions to the total $A_0(Q)$ due to static disorder (e.g., Mg^{2+} dopants), it was noted that this study is more sensitive to the $A_1(Q)$.

As shown in Figure 7c,d and detailed in the Supporting Information, from 400 to 550 K, the elastic and quasi-elastic amplitudes from scenario i with the T1T2R diffusion pathway had the best agreement with the empirical model amplitudes. However, from 600 to 650 K, amplitudes from scenario i for any of the three possible diffusion pathways had poor agreement with the empirical model amplitudes. This corresponded with a shift in both the amplitude and Q-dependence of the empirical $A_1(Q)$ between 550 and 600 K (Figure 5c). The relative amplitude of $A_1(Q)$ and $A_0(Q)$ indicates that this change is not from any increase in the fraction of sodium cations participating in long-range diffusion (see the Supporting Information). Therefore, the observed change at 600 K is more likely due to a change in the local rotational diffusion of the phosphate anions, which we propose corresponds to a gradual onset of the slow phosphate rotation in the manner of a mixed dynamical phase.

To test this, a mixing parameter y was added to account for the possibility of scenarios i and ii occurring simultaneously. Here, y denotes the fraction of the material where the phosphate anions undergo both the fast and slow rotations. Thus, an observable scattering function can be written as

$$(1-y)S(Q, \omega)^{\text{fast rotation only}} + yS(Q, \omega)^{\text{combined rotation}}$$

$$(4)$$

The amplitudes of the modified model in eq 4 were then fitted to the empirical model amplitudes at 600 and 650 K, with y and again a common scale factor as the free fitting parameters. Details are provided in the Supporting Information. As shown in Figure 8, this resulted in an improved fit to the empirical structure factors. The best agreement is achieved with having the majority phase (fast phosphate rotation only) follow the T1T2R pathway and the minority phase (combined phosphate rotation) as either T1T2R or T1RT1R. The significance of this result is that it is consistent with the preferred pathway from 400 to 550 K and the proposed pathways from the jump matrix model.

We note the presence of deviations between the experimental and model amplitudes at all temperatures, around 1.8 Å^{-1} and toward the lower Q region of the data. The deviations around 1.8 Å^{-1} correspond to dynamical Na−Na correlations[36] which were omitted for being negligible everywhere else, as explained at the beginning of the present analysis. The deviations present at lower Q correspond to correlations that are static on the time scale of our study, since those only show in the elastic amplitudes.

Finally, the activation energy associated with T1T2R sodium jump diffusion pathway in the absence of slow rotation (see the Supporting Information) was estimated. An Arrhenius fit of the residence times yields 0.34 ± 0.01 eV, which is consistent with the value of 0.376 eV obtained by *ab initio* molecular dynamics calculations for $Na_{2.5}Mg_{0.25}PO_4$ reported by Samiee et al.[16] These energies are also comparable with the reported activation energies of 0.38 ± 0.02 and 0.35 ± 0.01 eV for solid solution $xNa_2SO_4 \cdot (1 - x)Na_3PO_4$ for $x = 0.1$ and 0.5,
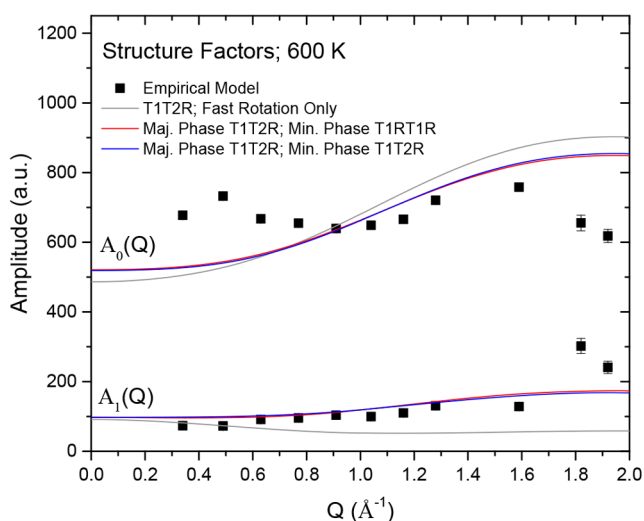
Figure 8. Comparison of the agreement between the $A_0(Q)$ and $A_1(Q)$ and the amplitudes of scenario i (fast rotation only) model for the T1T2R pathway (gray) and the mixed dynamical models for majority phase T1T2R, minority phase T1RT1R (red) and majority phase T1T2R, minority phase T1T2R (blue) at 600 K. Here, majority phase refers to the fraction of the material where the phosphate anions undergo the fast rotation only, while in the minority phase, the phosphate anions undergo both the fast and slow rotations.

respectively.[19] This result supports the finding that Mg^{2+} doping significantly lowers the activation energy for sodium long-range diffusion from 0.71 ± 0.04 eV in pure γ-Na_3PO_4.[16,19]

In summary, the approach of examining and modeling the scattering function in this work has provided the sensitivity to select a single preferred sodium long-range diffusion pathway, which was not possible from an *ad hoc* application of a uniform, long-range translational jump representation of the sodium dynamics. Moreover, the preference for the T1T2R diffusion pathway suggests dynamic coupling between the phosphate rotations and sodium long-range diffusion. Deviations of the model from the data are indicative of additional features of Mg^{2+}-stabilized γ-Na_3PO_4 that are not within the scope of this study being focused on sodium self-diffusion. Specifically, future work may aim to characterize collective sodium diffusion and specifically the impact of magnesium doping on sodium distribution. Indeed, the insight into the sodium self-diffusion mechanism influenced by the rotational diffusion on the phosphate anion framework presented in this study provides solid groundwork for the targeted characterization of the contributions that would improve the presented models.

4. CONCLUSIONS

This work has shown that Mg^{2+} stabilizes γ-Na_3PO_4 to temperatures as low as 4 K. As a rotor phase material, orientational disorder of the phosphate anions is evidenced by the Q-dependent diffuse scattering background in the NPD patterns and high values of thermal displacement parameters even at 4 K. Each phosphate group is bound to a sodium cation in a tetrahedral site which participates in the phosphate rotations. Therefore, it is necessary to distinguish any phosphate bound sodium from the remaining sodium in tetrahedral sites. In this work, we introduce two possible configurations of the phosphate binding to make this

distinction, which is not immediately clear from the average structure.

QENS broadening due to Na^+ long-range self-diffusion was modeled via a jump diffusion matrix construction. From this approach, we proposed two possible diffusion pathways: resCE and T1T2R. These pathways are dependent on the configuration of the phosphate-sodium binding, thus reflecting the strong coupling between a material's structure and dynamics. Examination of the elastic and quasi-elastic scattering amplitudes provided additional sensitivity in distinguishing between the proposed diffusion pathways. From this approach, the T1T2R pathway was found to be the preferred diffusion model. Significantly, this pathway strongly suggests a coupling between the rotational diffusion of the phosphate anion framework and sodium long-range diffusion. In addition, this analysis suggested that there is a gradual onset of the slow phosphate rotation at high temperatures, leading to the notion of a mixed dynamical phase.

■ ASSOCIATED CONTENT

ⓢ Supporting Information

The Supporting Information is available free of charge at https://pubs.acs.org/doi/10.1021/jacs.1c06905.

> Rietveld-refined fits, crystallographic tables, criteria for phosphate-bound sodium, types of sodium, QENS measurement times, fraction of localized sodium determination, derivation of the jump matrix, orientational averaging, fits to QENS spectra and fit parameters, derivation of rotational structure factors, conditions and derivation of the corrected scattering function, amplitudes for jumps, configurations and fits with the mixed dynamical phase, estimation of activation energy (PDF)

■ AUTHOR INFORMATION

Corresponding Authors

Ying Shirley Meng − *Department of NanoEngineering and Sustainable Power & Energy Center (SPEC), University of California, San Diego, La Jolla, California 92093, United States;* ⓞ orcid.org/0000-0001-8936-8845; Email: shmeng@ucsd.edu

Neeraj Sharma − *School of Chemistry, University of New South Wales Australia, Sydney, NSW 2052, Australia;* ⓞ orcid.org/0000-0003-1197-6343; Email: neeraj.sharma@unsw.edu.au

Nicolas R. de Souza − *Australian Nuclear Science and Technology Organisation, Kirrawee DC, NSW 2232, Australia;* Email: nds@ansto.gov.au

Authors

Emily A. Cheung − *School of Chemistry, University of New South Wales Australia, Sydney, NSW 2052, Australia*

Han Nguyen − *Department of NanoEngineering, University of California, San Diego, La Jolla, California 92093, United States*

Hanmei Tang − *Department of NanoEngineering, University of California, San Diego, La Jolla, California 92093, United States;* ⓞ orcid.org/0000-0003-2659-7768

Anton P. J. Stampfl − *Australian Nuclear Science and Technology Organisation, Kirrawee DC, NSW 2232, Australia*

Maxim Avdeev − *Australian Nuclear Science and Technology Organisation, Kirrawee DC, NSW 2232, Australia; School of Chemistry, The University of Sydney, Sydney 2006, Australia;* ⊙ orcid.org/0000-0003-2366-5809

■ REFERENCES

(1) Börjesson, L.; Torell, L. M. Reorientational motion in superionic sulfates: A Raman linewidth study. *Phys. Rev. B: Condens. Matter Mater. Phys.* **1985**, *32* (4), 2471−2477.

(2) Hruschka, H.; Lissel, E.; Jansen, M. Na-Ion conduction in the solid solutions of Na_3PO_4/Na_2SO_4 and Na_3AlF_6/Na_2SO_4. *Solid State Ionics* **1988**, *28*, 159−162.

(3) Jansen, M. Volume Effect or Paddle-Wheel Mechanism—Fast Alkali-Metal Ionic Conduction in Solids with Rotationally Disordered Complex Anions. *Angew. Chem., Int. Ed. Engl.* **1991**, *30* (12), 1547−1558.

(4) Wilmer, D.; Feldmann, H.; Lechner, R. E. Fast Cation Conduction and Anion Rotational Disorder in the High-Temperature Phase of Lithium Sodium Sulfate. *Z. Phys. Chem.* **2004**, *218*, 1439.

(5) Wilmer, D.; Funke, K.; Witschas, M.; Banhatti, R. D.; Jansen, M.; Korus, G.; Fitter, J.; Lechner, R. E. Anion reorientation in an ion conducting plastic crystal − coherent quasielastic neutron scattering from sodium ortho-phosphate. *Phys. B* **1999**, *266* (1), 60−68.

(6) Zhang, Z.; Zou, Z.; Kaup, K.; Xiao, R.; Shi, S.; Avdeev, M.; Hu, Y.-S.; Wang, D.; He, B.; Li, H.; Huang, X.; Nazar, L. F.; Chen, L. Correlated Migration Invokes Higher Na+-Ion Conductivity in NaSICON-Type Solid Electrolytes. *Adv. Energy Mater.* **2019**, *9* (42), 1902373.

(7) Hooper, A.; McGeehin, P.; Harrison, K. T.; Tofield, B. C. Ionic conductivity of pure and doped Na3PO4. *J. Solid State Chem.* **1978**, *24* (3), 265−275.

(8) Newsam, J. M.; Cheetham, A. K.; Tofield, B. C. Structural studies of the high-temperature modifications of sodium and silver orthophosphates, $II-Na_3PO_4$ and $II-Ag_3PO_4$, and of the low-temperature form $I-Ag_3PO_4$. *Solid State Ionics* **1980**, *1* (5), 377−393.

(9) Harrison, R. J.; Putnis, A.; Kockelmann, W. Phase transition behaviour and equilibrium phase relations in the fast-ion conductor system $Na_3PO_4-Na_2SO_4$. *Phys. Chem. Chem. Phys.* **2002**, *4* (14), 3252−3259.

(10) Belik, A. A.; Ivanov-Shitz, A. K.; Bykov, A. B.; Verin, I. A.; Golubev, A. M.; Nistyuk, A. V. Structure and electric conductivity of Na_3PO_4 single crystals. *Crystallogr. Rep.* **2000**, *45* (6), 902−906.

(11) Wiench, D. M.; Jansen, M. Über Na_3PO_4: Versuche zur Reindarstellung, Kristallstruktur der Hochtemperaturform [1]. *Z. Anorg. Allg. Chem.* **1980**, *461* (1), 101−108.

(12) Irvine, J. T. S.; West, A. R. Solid electrolytes based on $Na_3PO_4:M^{4+}$ (M = Zr, Hf, Ti, Sn, Ce, Th). *J. Solid State Chem.* **1988**, *74* (2), 385−392.

(13) Irvine, J. T. S.; West, A. R. Solid electrolytes based on Na_3PO_4 doped with S, Se, Mo, W. *Mater. Res. Bull.* **1987**, *22* (8), 1047−1054.

(14) Irvine, J. T. S.; West, A. R. Solid electrolytes based on $Na_3PO_4:M^{2+}$ (M = Mg, Zn, Ca, Sr). *Solid State Ionics* **1989**, *37* (1), 73−78.

(15) Milne, S. J.; West, A. R. Zr-doped Na_3PO_4: Crystal chemistry, phase relations, and polymorphism. *J. Solid State Chem.* **1985**, *57* (2), 166−177.

(16) Samiee, M.; Radhakrishnan, B.; Rice, Z.; Deng, Z.; Meng, Y. S.; Ong, S. P.; Luo, J. Divalent-doped $Na_3Zr_2Si_2PO_{12}$ natrium superionic conductor: Improving the ionic conductivity via simultaneously optimizing the phase and chemistry of the primary and secondary phases. *J. Power Sources* **2017**, *347*, 229−237.

(17) Wang, B.; Greenblatt, M. Ionic conductivities of $Na_4MgP_2O_8$ and partially substituted $Na_{4+x}MgP_{2-x}Si_xO_8$ solid solutions. *Solid State Ionics* **1993**, *59* (3), 243−247.

(18) Yin, W.-G.; Liu, J.; Duan, C.-G.; Mei, W. N.; Smith, R. W.; Hardy, J. R. Superionicity in Na_3PO_4: A molecular dynamics simulation. *Phys. Rev. B: Condens. Matter Mater. Phys.* **2004**, *70* (6), 064302.

(19) Wilmer, D.; Combet, J. Sodium ion diffusion in solid solutions of sodium orthophosphate and sodium sulphate. *Chem. Phys.* **2003**, *292* (2), 143−152.

(20) Bee, M. *Quasielastic Neutron Scattering. Principles and Applications in Solid State, Chemistry, Biology and Materials Science*; Adam Hilger: 1988.

(21) Zhang, Z.; Roy, P.-N.; Li, H.; Avdeev, M.; Nazar, L. F. Coupled Cation−Anion Dynamics Enhances Cation Mobility in Room-Temperature Superionic Solid-State Electrolytes. *J. Am. Chem. Soc.* **2019**, *141* (49), 19360−19372.

(22) Zhang, Z.; Li, H.; Kaup, K.; Zhou, L.; Roy, P.-N.; Nazar, L. F. Targeting Superionic Conductivity by Turning on Anion Rotation at Room Temperature in Fast Ion Conductors. *Matter* **2020**, *2* (6), 1667−1684.

(23) Pramanik, K.; Sau, K.; Kumar, P. P. Role of Framework Flexibility in Ion Transport: A Molecular Dynamics Study of $LiM_2V(PO_4)_3$. *J. Phys. Chem. C* **2020**, *124* (7), 4001−4009.

(24) Sau, K.; Ikeshoji, T. Origin of Fast Ion Conduction in Na_3PS_4: Insight from Molecular Dynamics Study. *J. Phys. Chem. C* **2020**, *124* (38), 20671−20681.

(25) Sau, K.; Ikeshoji, T.; Kim, S.; Takagi, S.; Orimo, S.-i. Comparative Molecular Dynamics Study of the Roles of Anion−Cation and Cation−Cation Correlation in Cation Diffusion in $Li_2B_{12}H_{12}$ and $LiCB_{11}H_{12}$. *Chem. Mater.* **2021**, *33* (7), 2357−2369.

(26) Liss, K.-D.; Hunter, B.; Hagen, M.; Noakes, T.; Kennedy, S. Echidna—the new high-resolution powder diffractometer being built at OPAL. *Phys. B* **2006**, *385−386*, 1010−1012.

(27) Avdeev, M.; Hester, J. R. ECHIDNA: a decade of high-resolution neutron powder diffraction at OPAL. *J. Appl. Crystallogr.* **2018**, *51* (6), 1597.

(28) Wallwork, K. S.; Kennedy, B. J.; Wang, D. The High Resolution Powder Diffraction Beamline for the Australian Synchrotron. *AIP Conf. Proc.* **2006**, *879* (1), 879−882.

(29) Larson, A. C.; Von Dreele, R. B. *General Structure Analysis System (GSAS)*; Los Alamos National Laboratory: 2004.

(30) Toby, B. H. EXPGUI, a graphical user interface for GSAS. *J. Appl. Crystallogr.* **2001**, *34*, 210−213.

(31) de Souza, N. R.; Klapproth, A.; Iles, G. N. EMU: high-resolution backscattering spectrometer at ANSTO. *Neutron News* **2016**, *27*, 20−21.

(32) Wilmer, D.; Feldmann, H.; Combet, J.; Lechner, R. E. Ion conducting rotor phases—new insights from quasielastic neutron scattering. *Phys. B* **2001**, *301* (1), 99−104.

(33) Wilmer, D.; Feldmann, H.; Lechner, R. E. Ion dynamics in solid solutions of sodium phosphate and sodium sulfate. *Phys. Chem. Chem. Phys.* **2002**, *4* (14), 3260−3265.

(34) Witschas, M.; Eckert, H. ^{31}P and ^{23}Na Solid-State NMR Studies of Cation Dynamics in HT-Sodium Orthophosphate and the Solid Solutions $(Na_2SO_4)_x-(Na_3PO_4)_{1-x}$†. *J. Phys. Chem. A* **1999**, *103* (50), 10764−10775.

(35) Springer, T. Quasielastic neutron scattering for the investigation of diffusive motions in solids and liquids. In *Springer Tracts in Modern Physics*, Vol. *64*, Springer: 1972; pp 1−100.

(36) Hempelmann, R. *Quasielastic Neutron Scattering and Solid State Diffusion.*; Oxford University Press: Oxford, 2000.

(37) Sears, V. F. Neutron scattering lengths and cross sections. *Neutron News* **1992**, *3* (3), 26−37.

(38) Hempelmann, R.; Richter, D.; Faux, D.; Ross, D. Collective relaxation, single particle motion and short range order in α-NbD$_x$: A quasielastic neutron scattering study. *Z. Phys. Chem.* **1988**, *159*, 175−184.

(39) Ross, D. K.; Wilson, D. L. T. The Use of Monte Carlo Calculations in the Prediction of Quasi-Elastic Neutron Scattering from Atoms Diffusing in Periodic Lattices. In *Neutron Inelastic Scattering*; IAEA: Vienna, 1977; Vol. *2*, pp 383−397.

(40) Sinha, S. K.; Ross, D. K. Self-consistent density response function method for dynamics of light interstitials in crystals. *Physica B+C* **1988**, *149* (1-3), 51−56.

(41) Cook, J. C.; Richter, D.; Hempelmann, R.; Ross, D. K.; Züchner, H. Quasi-elastic neutron scattering studies of collective and correlated tracer diffusion in the systems α'-NbD$_x$ and α'-NbH$_x$. *J. Less-Common Met.* **1991**, *172−174*, 585−594.

(42) Coddens, G. Coherent quasielastic neutron scattering: A theorem about total neutron scattering functions for rotational jump diffusion of molecules on a lattice. *Phys. Rev. B: Condens. Matter Mater. Phys.* **2001**, *63* (6), 064105.

(43) Blaesser, G.; Peretti, J. In *International Conference on Vacancies and Interstitials in Metals*; Seeger, A., Schaumader, D., Schilling, W., Drehl, J., Eds.; North-Holland Publishing: Jülich, 1968; Vol. *2*, p 886.

(44) Rowe, J. M.; Sköld, K.; Flotow, H. E.; Rush, J. J. Quasielastic neutron scattering by hydrogen in the α and β phases of vanadium hydride. *J. Phys. Chem. Solids* **1971**, *32* (1), 41−54.

(45) Randl, O. G.; Sepiol, B.; Vogl, G.; Feldwisch, R.; Schroeder, K. Quasielastic Mossbauer spectroscopy and quasielastic neutron scattering from non-Bravais lattices with differently occupied sublattices. *Phys. Rev. B: Condens. Matter Mater. Phys.* **1994**, *49* (13), 8768−8773.

(46) Chudley, C. T.; Elliott, R. J. Neutron Scattering from a Liquid on a Jump Diffusion Model. *Proc. Phys. Soc., London* **1961**, *77* (2), 353.

(47) Witschas, M.; Eckert, H.; Wilmer, D.; Banhatti, R. D.; Funke, H.; Fitter, J.; Lechner, R. E.; Korus, G.; Jansen, M. Anion Rotation and Cation Transport in the Rotor Phase α-Sodium Orthophosphate: Paddle-Wheel Mechanism Redefined in View of New Experimental Results. *Z. Phys. Chem.* **2000**, *214*, 643.